Design Procedure for Interdigital Waveguide Bandpass Filters based on Flat Metallic Strips

R. García[1], A. A. San-Blas[1], S. Bonte[1], A. Coves[1], M. A. Sánchez-Soriano[2], M. Guglielmi[3], V. E. Boria[3]

[1]Department of Communications Engineering-I3E, Miguel Hernández University of Elche, Spain
[2]Department of Physics, Systems Engineering and Signal Theory, University of Alicante, Spain
[3]Department of Communications-iTEAM, Technical University of Valencia, Spain

Key Points:

- A new topology for interdigital bandpass filters based on flat metallic strips is proposed
- A systematic procedure based on the segmentation of the component is presented for the efficient design of the proposed interdigital bandpass filters
- A power handling capability study of the designed interdigital filters is performed

Corresponding author: Ángel A. San-Blas, aasanblas@umh.es

Abstract

In this work, we describe a new topology for interdigital bandpass filters implemented in waveguide technology. Compared to classical coaxial resonators, which are typically based on cylindrical metallic posts, the resonators that we propose are based on rectangular boxed cavities loaded with flat metallic strips of a finite thickness. The main advantages of the proposed topology are low-cost practical realization and manufacture simplicity. The design process, which is based on the classical circuit-based approach combined with an efficient segmentation of the component, uses the well-known Aggressive Space Mapping technique, with the aim of reducing the overall computation effort. In order to validate the new topology and the design procedure, interdigital bandpass filters of orders 3 and 5 operating at the S-band have been designed. For validation purposes, the results obtained are successfully compared to simulations provided by two different full-wave electromagnetic tools (i.e., Ansys HFSS and CST Studio Suite). Furthermore, a multipactor study has also been performed, with the aim of exploring the power handling capability of the proposed filters in view of possible space applications. Finally, the design of classical interdigital filters based on cylindrical posts is also discussed, with the aim of comparing both topologies regarding compactness, as well as in terms of their electrical and high-power performance.

1 Introduction

Bandpass filters based on coaxial resonators, such as filters in combline or interdigital configuration implemented in waveguide technology, are commonly used in multiple applications, including space and wireless communications systems (Wang & Yu, 2009), (García et al., 2018), (Macchiarella et al., 2018), (Bastioli et al., 2018), (Vallerotonda et al., 2019), (Tamiazzo, 2021), (Zeng et al., 2022), (Yan et al., 2024). Classically, resonators based on rectangular cavities loaded with metallic posts of cylindrical (J. Li et al., 2018), (Boni et al., 2023) or rectangular/square geometry (Arndt & Brandt, 2002), (Kong et al., 2023) have been used in this type of coaxial resonator filters. Other more complex topologies have also been investigated in the past, as the interdigital bandpass filter designed in (Venter et al., 2020), where resonator posts with a triangular cross-section were proposed. Generally, coaxial resonators are coupled by using irises of rectangular geometry, whose position in the structure determines the type of coupling (electric or magnetic) (Jamshidi-Zarmehri et al., 2023), (Zeng et al., 2023). On the other hand, inter-resonator coupling can also be controlled by designing the separation between the posts, without the need to insert irises in the component (Z. Li et al., 2023), (Macchiarella et al., 2023).

Regarding the state-of-the-art of interdigital bandpass filters based on cylindrical posts, an in-line topology was presented in (Ikram & Rana, 2006), where a fifth-order Chebyshev interdigital bandpass filter operating at C-band was designed. Moreover, a manifold cavity diplexer operating at L-band was designed in (Packiaraj et al., 2005), while a low-loss triplexer that used a combination of a microstrip star junction and three interdigital bandpass filters was proposed in (Munina & Turalchuk, 2015). More recently, a Ku-band 8th-order interdigital filter with an in-line configuration was presented in (J. Li et al., 2018).

On the other hand, resonators based on rectangular or square posts have also been widely used in interdigital waveguide filters. For instance, an interdigital cavity filter operating at Ku-band is designed in (Wu et al., 2019), where two transmission zeros are realized in the frequency response by considering additional resonators outside of the ports of the filter. A further example of an interdigital filter using posts with a rectangular geometry can be found in (Jiang et al., 2019), where an eighth-order filter with an improved stop-band suppression is designed. Moreover, a wideband waveguide diplexer based on interdigital filters for mobile base stations is proposed in (Kobrin et al., 2019). Another interesting contribution was presented in (Anand, 2021), where a folded configuration for interdigital filters was proposed in order to implement cross-couplings between the resonators. Additive manufacturing techniques have also been used for designing interdigital filters for radar applications (Rodriguez-Morales et al., 2021), and satellite communication systems (Venter et al., 2020). More recently, a miniaturized interdigital cavity filter using loading capacitors is investigated in (Kong et al., 2023). In general, the design process for the bandpass filters presented in the contributions discussed above, is based on the classical approach proposed in (Cameron et al., 2018), so, regardless of the filter order, all the relevant dimensions of the component are optimized at the same time, thus requiring a great computational effort to complete the design process.

In this work, a new topology of waveguide bandpass filters based on coaxial resonators implemented in an interdigital configuration is presented. The main novelty of the proposed in-line filter consists in the use of cavities loaded with planar metallic strips of a finite thickness, as shown in Fig. 1, where a third-order interdigital bandpass filter is depicted. A major advantage of this new topology lies in the fact that the filters could be manufactured using low-cost and more simple realization techniques. For instance, the whole structure can be implemented through the cascaded connection of simpler rectangular waveguide sections (including the flat strips), each one manufactured with a CNC (computer numerical control) milling technique. The design procedure that we propose combines the use of the classical circuit-based approach (Cameron et al., 2018) with a strategy based on a segmentation of the structure (San-Blas et al., 2021), (Jamshidi-Zarmehri et al., 2023).

In the suggested design procedure, input and output resonators are first designed to achieve the desired external quality factor. After that, the coupling between adjacent resonators is addressed, with the aim of achieving a set of initial values for the physical dimensions of the structure. To continue, and specially for high-order filters, a systematic design procedure based on the segmentation of the whole component is proposed. In this procedure, the different resonators of the filter are added one after the other, thus dividing the design process in more simple steps, while also reducing the number of variables to be optimized in each stage. Equivalent circuit models are also important in this approach, since their electrical responses will be used as target curves in all optimization stages of the design procedure. Furthermore, the Aggressive Space Mapping (ASM) technique (Bandler et al., 1995) has also been used in this work, so that most of the optimizations performed during the design process are carried out very efficiently in a low-precision simulation space (the coarse model).

In order to validate the new topology that we propose, two interdigital bandpass filters operating at S-band have been designed. The correct electrical performance of the filters is successfully validated using two different electromagnetic (EM) simulation tools (Ansys HFSS, and CST Studio Suite). In addition, a multipactor study (Berenguer et al., 2019) is also performed for both filters, in order to evaluate the high-power performance of this new topology under high-vacuum conditions. Furthermore, the design of classical interdigital filters based on cylindrical posts is also discussed, with the aim of comparing both topologies in terms of compactness, electrical performance and power handling capability.

2 Design of the coaxial resonator and related equivalent circuit

The basic coaxial resonator proposed in this work is shown in Fig. 2. It is based on a rectangular cavity loaded with a thick metallic strip. The strip is connected to the base of the resonator at one end. At the other end, there is an open circuit or gap, as shown in Fig. 2. In addition, the metal strip is located in the center of the rectangular enclosure. The relevant dimensions of the resonator are designed with the objective of having a resonance at the center frequency f_0 of the filter. In this work, two bandpass

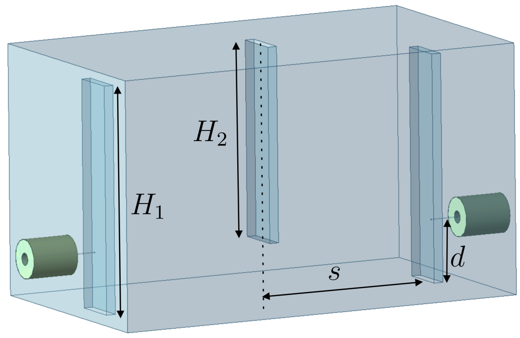

Figure 1. Third-order symmetric interdigital bandpass filter with flat metallic strips.

filters of orders $N=3$ and $N=5$ will be designed. Since both of them share the same center frequency (f_0 = 3 GHz), the resonator designed in this section will be used in both bandpass filters.

In order to design the resonator, the full-wave EM simulator Ansys HFSS has been used. First of all, an access port located at the $y=0$ plane of the structure in Fig. 2, has been opened. It is important to note that, with this access port, the resonator becomes a section of coaxial guide, with internal and external rectangular contours, loaded by a length of short-circuited rectangular waveguide. To continue, the phase of the S_{11} parameter at the input port is calculated, and the dimensions of the resonator are optimized until the phase of S_{11} is equal to 180° at a frequency equal to f_0. The final dimensions (all expressed in mm) of the optimized resonator are as follows (see Fig. 2): $a_r = b_r = 26$, $l_r = 7$, $H = 23.233$, $w = 5$ and $t = 1$. It is important to note that the dimensions a_r, b_r, l_r (dimensions of the rectangular enclosure), w and t (width and thickness of the strip) will remain fixed, and will not be optimized during the filter design process.

In addition, we are also interested in obtaining an equivalent circuit of the resonator based on lumped elements. This equivalent circuit consists of a series combination of an inductance L and a capacitor C. With the aim of obtaining the equivalent series network, the slope parameter X of the optimized coaxial resonator is first calculated from the simulated results (Matthaei et al., 1980):

$$X = \frac{w_0}{2} \left. \frac{dX_{in}(w)}{dw} \right|_{w=w_0} = 295.48\,\Omega \tag{1}$$

where $w_0 = 2\pi f_0$, and X_{in} represents the reactance of the input impedance of the optimized resonator. Then, the value of the equivalent inductance of the resonator can be calculated as: $L = X/w_0 = 15.676$ nH. The value of the equivalent capacitance can now be computed using: $C = 1/(w_0^2 L) = 0.179$ pF.

The unloaded Q factor of the designed resonator has been calculated using Ansys HFSS. In this analysis, an equivalent conductivity value of $38 \cdot 10^6$ S/m (aluminium) has been considered, thus obtaining $Q_u = 1462$. Furthermore, we have computed both the unloaded Q factor and the resonant frequency (f_0) of the designed resonator in terms of the height H of the strip, and also as a function of the length l_r of the rectangular enclosure. The obtained results are shown in Fig. 3. As we expected, when the height of the strip decreases (thus increasing the gap between the strip and the top wall of the enclosure), both Q_u and f_0 increase (see Fig. 3, left). As it is well known, the cited gap represents a critical region in terms of high-power performance in classical coaxial resonator filters. Nevertheless, since the thickness of the strip used in our proposed resonator

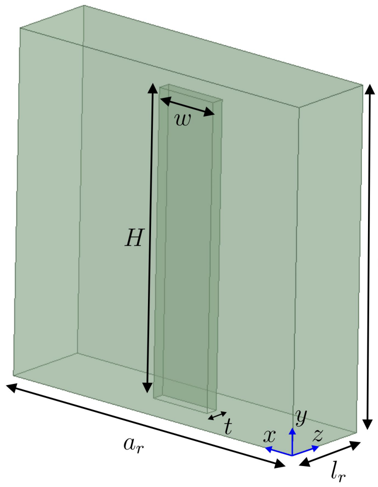

Figure 2. Coaxial resonator loaded with a flat metallic strip.

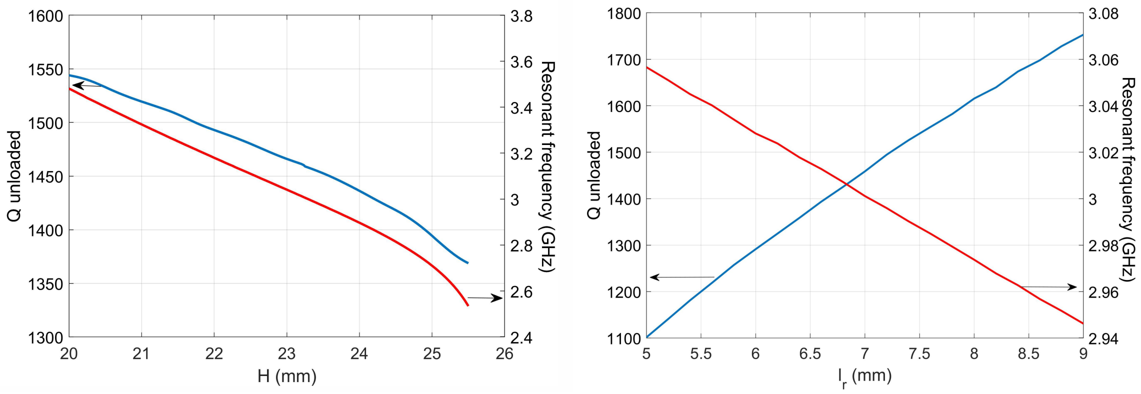

Figure 3. Variation of the unloaded Q factor and the resonant frequency of the flat strip resonator in terms of H and l_r.

is small (only 1 mm), the equivalent capacitance in this region is less significant than the one found in classical resonators based on cylindrical posts. Therefore, an increased high-power performance is expected compared to classical interdigital filters, as it is discussed in Section 6.

On the other hand, as it can be observed in Fig. 3 (right), when the length of the rectangular enclosure decreases (thus obtaining a more compact resonator), Q_u decreases (thus increasing the losses, as well), while f_0 increases. Furthermore, for comparison purposes, we have also analysed the unloaded Q factor of a classical resonator loaded with a cylindrical post. In this design, the post diameter has been chosen to be equal to the width w of the flat strip, while the dimensions of the rectangular enclosure are the same that we have used in the flat strip resonator. The computed Q factor is $Q_u = 937$, so the novel resonator proposed in our work has a better performance in terms of losses than the classical solution based on cylindrical posts.

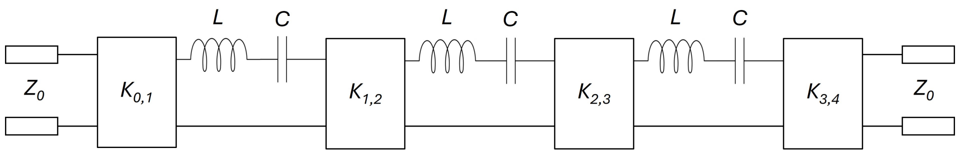

Figure 4. Equivalent circuit network of the 3rd-order interdigital bandpass filter.

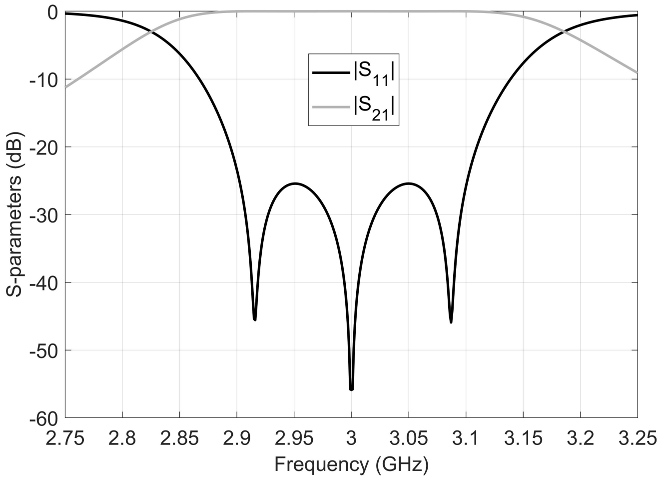

Figure 5. Frequency response of the equivalent circuit network shown in Fig. 4.

3 Equivalent circuit of the bandpass filters

The purpose of this section is to obtain an equivalent network to characterize the designed bandpass filters. The electrical response of this equivalent circuit will be used to generate target curves to obtain the in-band response of the designed filter using iterative optimizations. The equivalent circuit of the filters will be composed of the cascade connection of ideal impedance inverters (which will characterize both the input/output couplings and also the inter-resonator couplings) and series L-C networks (which will model the resonators). It is also worth noting that, as it is well known, transmission zeros cannot be realized using coaxial resonators in a standard in-line interdigital configuration.

The electrical specifications for the 3rd-order interdigital filter that will be designed in Section 4 are: center frequency $f_0 = 3$ GHz, return loss of $RL = 25$ dB, and bandwidth $BW = 200$ MHz. Given these specifications, the values (in Ω) of the impedance inverters, which have been calculated using the slope parameter X of the resonator, are as follows: $K_{01} = K_{34} = 86.394$ and $K_{12} = K_{23} = 24.027$ (Matthaei et al., 1980). The equivalent circuit of the 3rd-order filter is shown in Fig. 4, while its frequency response is displayed in Fig. 5.

4 Design of a 3rd-order bandpass filter following a classical approach

In this section, the procedure used to design a third-order Chebyshev bandpass filter (electrical specifications: $f_0 = 3$ GHz, $RL = 25$ dB, $BW = 200$ MHz) is described in detail. As we have previously mentioned, in this case, where the order of the filter is not high, the design process is based on the classical approach proposed in (Cameron et al., 2018). First, input and output couplings are characterized and, after that, the inter-resonator couplings are calculated. Finally, the complete filter is assembled and all di-

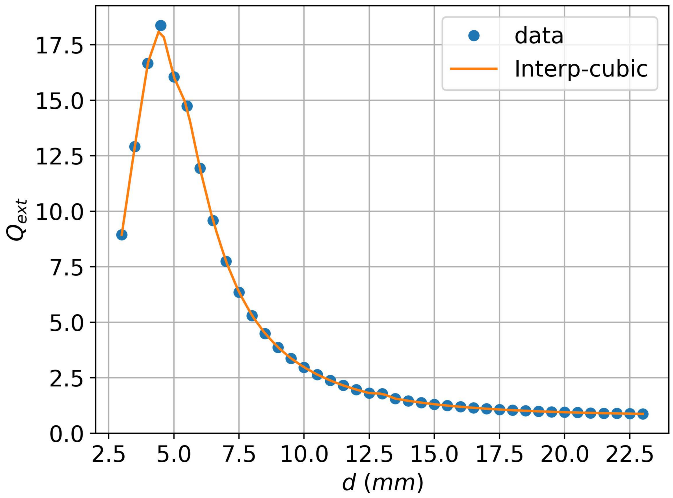

Figure 6. External quality factor in terms of the distance d.

mensions are optimized using as a target the response of the corresponding equivalent circuit (see Fig. 5).

First, the design of the excitation of the input and output resonators is discussed. These resonators are fed with SMA coaxial waveguides ($\epsilon_r = 2.2$), with external and internal radii of 2.05 and 0.65 mm, respectively. The metallic strips of the input/output resonators are in contact with a metal feeding probe, located at a distance d from the bottom of the cavity, as shown in Fig. 1. The distance d will be optimized in order to obtain the required external quality factor Q_{ext}. This parameter can be obtained following the method detailed in (Cameron et al., 2018), namely, by evaluating the group delay of parameter S_{11} at frequency f_0. Fig. 6 shows the dependence of the external quality factor in terms of the distance d. On the other hand, the required value for Q_{ext} can be calculated as follows (Cameron et al., 2018):

$$Q_{ext} = \frac{f_0}{BWm_{01}^2} = 10.055 \tag{2}$$

where $m_{01} = 1/\sqrt{g_0 g_1}$ (being g_0 and g_1 the corresponding low-pass prototype elements). Furthermore, Q_{ext} is related to K_{01} through $Q_{ext} = (XZ_0)/K_{01}^2$, where $Z_0 = \eta_0/\sqrt{\epsilon_r} =$ 253.9 Ω represents the modal impedance of the TEM mode of the coaxial waveguide port. In view of the value obtained for the required external quality factor, an initial value $d =$ 7.321 mm can be deduced from Fig. 6.

Once the couplings of the input/output resonators have been obtained, the couplings between adjacent resonators are characterized as a function of the spacing s between the strips (see Fig. 1). For this purpose, a symmetrical two-port component is considered, consisting of two resonators weakly coupled to the input and output coaxial ports. It is well known that the resonant frequencies of this component are related to the value of the electromagnetic coupling k of the structure, which can be obtained as a function of the separation s between strips, as shown in Fig. 7. Since the required value for the electromagnetic coupling between resonators #1 and #2 can be computed as $k_{12} = K_{12}/(w_0 L) =$ 0.0813, an initial value of $s = 14.774$ mm can be deduced from Fig. 7.

At this point, it would be interesting to determine the nature of the coupling (electric or magnetic) between two interdigital resonators based on flat metallic strips. First,

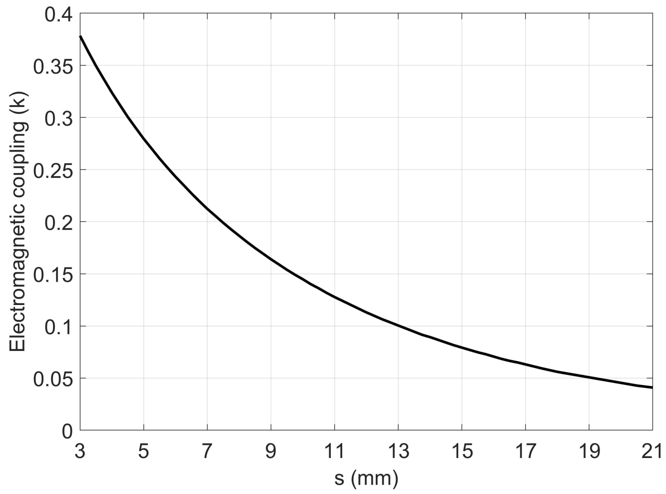

Figure 7. Electromagnetic coupling between adjacent resonators as a function of the separation s between strips.

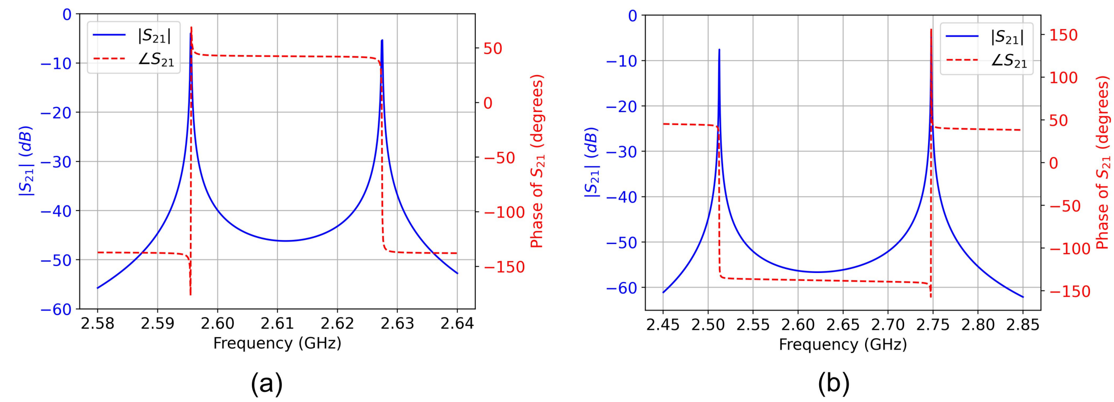

Figure 8. Magnitude and phase of the S_{21} parameter when the resonators are in (a) a combline configuration and in (b) an interdigital configuration.

let us consider two resonators coupled in a combline configuration, both weakly coupled to the coaxial input/output ports (the dimensions of the strips and the dimensions of the resonator have been deduced in Section 2). In this component, note that both resonator strips are connected to the bottom of the filter. In addition, a separation of $s =$ 14 mm between the resonators has been used for this simulation. It is well-known that, in this type of structure, the nature of the predominant coupling is magnetic (Thomas, 2003). Moreover, Fig. 8(a), which can be used to determine the magnitude of the electromagnetic coupling k (Cameron et al., 2018), shows the magnitude and the phase of the S_{21} parameter of the considered combline structure. On the other hand, Fig. 8(b) shows this same information when the two resonators are in an interdigital configuration. As we can observe, there is a phase shift of 180° between the S_{21} phase responses of the two cases analyzed, thus confirming a change in the sign of the predominant coupling. In this regard, it is important to note that the combline-type coupling (of magnetic nature) is approximately one order of magnitude lower than the interdigital one for the same resonator separation, thus making the non-adjacent couplings negligible in the interdigital case and, thereby, facilitating the proposed systematic in-line design.

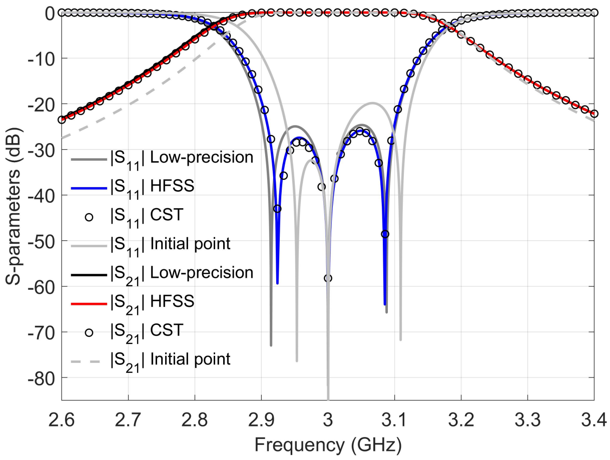

Figure 9. S-parameters of the designed 3rd-order interdigital filter. Comparison of results obtained with Ansys HFSS and CST Studio Suite.

In the next step of the design process, the complete filter is assembled (considering symmetry in the component) and the filter dimensions H_1, H_2, s and d (see Fig. 1) are optimized in a low-accuracy space, until recovering the target response. The values obtained are (all in mm) $H_1 = 23.380$, $H_2 = 20.144$, $s = 18.606$ and $d = 5.491$. All simulations previously described have been performed using the full-wave EM tool FEST3D (which is part of CST Studio Suite), with a set of parameters chosen to obtain very fast low-accuracy results. For instance, only 10 accessible modes (Conciauro et al., 2000) were considered in all simulations concerning the design process of this filter. Consequently, the resulting low-accuracy frequency response is not sufficiently precise for fabrication purposes. However, the well-known ASM technique presented in (Bandler et al., 1995) allows us to refine these results by transforming the low-accuracy data (coarse model) into a high-precision solution (fine model). In this design, FEST3D serves as the coarse model, while the finite-element EM tool Ansys HFSS is used as the fine model. In most cases, only a few iterations are required to obtain the target frequency response of the filter in the fine space.

The final dimensions obtained with the ASM procedure (in mm) are as follows: $H_1 = 23.683$, $H_2 = 20.320$, $s = 17.721$ and $d = 6.076$. In order to further validate both the topology of the new filter and the design procedure we have followed, the filter has been analyzed using an additional EM simulator, namely, CST Studio Suite. The results obtained are shown in Fig. 9, where an excellent agreement between the results provided by HFSS and CST can, indeed, be observed. We have also included in the same figure the S-parameters of the filter designed in the low-precision space to show that a very good agreement between the results obtained in both simulation spaces (low and high-precision models) has been achieved. Furthermore, the response in the fine space with the optimum dimensions found in the coarse space has also been included in Fig. 9 for comparison purposes (see label "Initial point").

At this point, it is important to discuss the design of classical interdigital filters based on cylindrical posts, with the aim of comparing this classical topology to the novel proposed flat strip configuration, both in terms of compactness and electrical performance. In this context, we have first designed a resonator ($f_0 = 3$ GHz) loaded with a cylindrical post whose diameter is equal to the width w of the flat strip that we have used in our previous design (the dimensions of the rectangular enclosure used in this resonator can be found in Section 2). Afterwards, the inter-resonator couplings have been com-

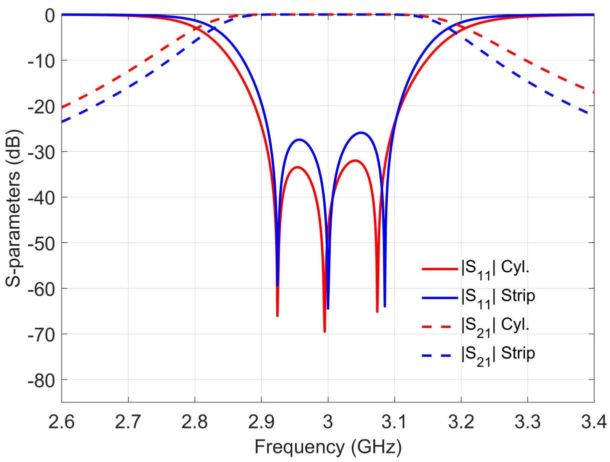

Figure 10. Electrical responses of the designed 3rd-order interdigital bandpass filters based on cylindrical posts and flat strips.

puted to determine the initial values for the different separations between resonators. Our results show that such initial values are very similar to the ones obtained when resonators based on flat strips are considered. We can, therefore, estimate that the final filter lengths for both considered topologies are comparable, so the compactness of our novel filter topology based on flat strips resonators is very similar to the one obtained with classical resonators loaded with cylindrical posts.

To validate this statement, a 3rd-order interdigital bandpass filter including resonators based on cylindrical posts has been designed following the approach previously detailed. The only difference is that, in this case, after computing the initial values for all relevant filter dimensions, a brute-force optimization algorithm has been used (instead of the ASM technique) in order to obtain the filter dimensions in a high-precision space. In this design, we have used the same coaxial excitation and the same electrical specifications that we employed for the 3rd-order filter based on flat strips. The dimensions of this filter (all in mm) are: $H_1 = 22.70$, $H_2 = 19.56$, $s = 18.54$ and $d = 5.40$, where s represents the separation between the centres of the cylindrical posts (see also Fig. 1 for the definition of these variables by considering cylindrical posts). The total length of the designed filter (high-precision space) is 44.1 mm, while the length of the 3rd-order filter based on flat strips previously designed is equal to 44.4 mm, thus confirming that both topologies exhibit an almost identical performance in terms of compactness. The in-band frequency responses (obtained using Ansys HFSS) of both 3rd-order filter topologies are shown in Fig. 10.

Regarding the insertion loss, we have considered a finite conductivity of $38 \cdot 10^6$ S/m (aluminium) in our analysis, and we have obtained that the insertion loss mean value is equal to 0.1 dB in the nominal passband ($2.9 - 3.1$ GHz) for both topologies. It is important to note at this point that, although the two filters have been designed with the same electrical specifications, the bandwidth of the filter based on cylindrical posts gets slightly higher than the bandwidth of the filter based on flat strips (see also Fig. 10). This fact explains why both filters present a very similar insertion loss, even though the resonator based on flat strips exhibits a higher unloaded Q factor.

We have also calculated the insertion loss of the 5th-order interdigital filter based on flat strips presented in the next section. In this case, the mean value in the nominal passband is of 0.24 dB. It is worth noting that the obtained values are consistent with

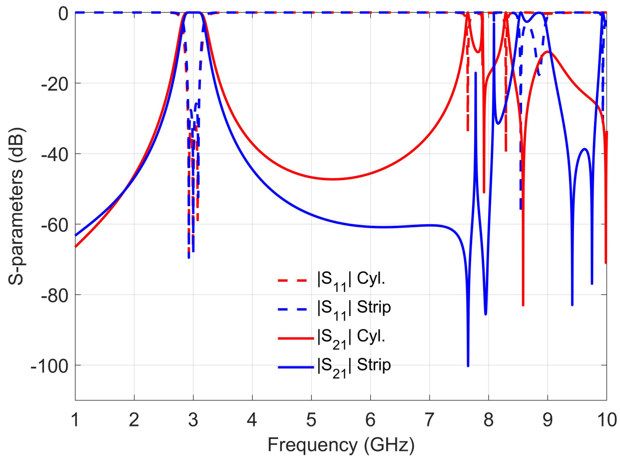

Figure 11. Broadband response of the designed 3rd-order interdigital bandpass filters.

the theoretical insertion loss computed using the analytical formulas found in the technical literature for the prescribed specifications.

On the other hand, and regarding the broadband performance, Fig. 11 shows the out-of-band response of the designed 3rd-order interdigital filter based on cylindrical posts (red lines) compared to the response of the filter based on flat strips (blue lines). It is worth mentioning that the interdigital filter based on flat strips shows an out-of-band rejection starting at higher frequencies, and a wider spurious-free range, when compared to the classical filter based on cylindrical posts. Therefore, the novel topology proposed in this work enhances the out-of-band performance of classical interdigital filters.

As we have mentioned before, a 3rd-order interdigital bandpass filter including resonators based on cylindrical posts has been designed using a brute-force algorithm to obtain the filter dimensions in a high-precision space. In particular, after obtaining an initial set of filter dimensions following the classical design approach, the whole component is assembled. Next, by means of a full-wave simulator (Ansys HFSS), the dimensions of the physical structure are iteratively optimized until the desired electrical response is recovered. Proceeding in this way, the complete set of the filter dimensions (4 dimensions in this case) is optimized at the same time. Compared to the design strategy based on the ASM technique, the design approach based on a brute-force design algorithm spends, approximately, 19% more computational time. In addition, it is worth noting that this conclusion stands for a third-order interdigital filter. Therefore, if a high-order filter needs to be designed, the number of involved physical dimensions will be higher and the cited increase in CPU time could be even more significant, since the brute-force algorithm does not benefit from the segmentation technique proposed in this work.

5 Design of a 5th-order bandpass filter using a segmentation technique

In this section, the design of a fifth-order interdigital bandpass filter with a Chebyshev response is addressed. The technique proposed for the efficient design of this high-order filter is based on a segmentation of the component, where the different resonators of the filter are progressively added one after the other, with the aim of reducing the number of variables to be optimized in each step of the design process. The electrical response (i.e., the group delay of the S_{11} parameter) of the equivalent circuit of the structure used in each step, will be used as the target curve in the optimization process. After that, the

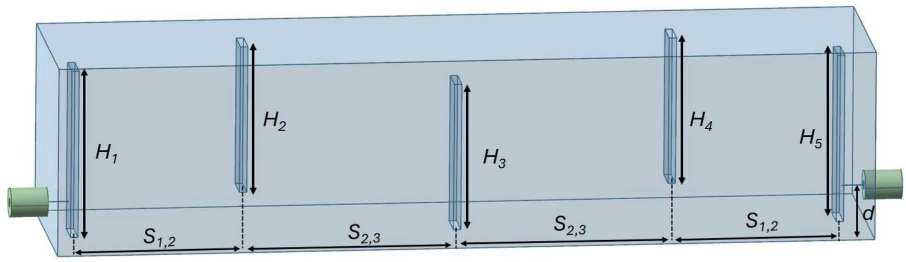

Figure 12. Fifth-order interdigital bandpass filter with flat metallic strips.

ASM technique will be used again to obtain the final dimensions. Fig. 12 shows the topology of the 5th-order filter under consideration.

The center frequency chosen for this bandpass filter is the same as the one we used for the 3rd-order filter. Therefore, both the resonator dimensions and the values of the equivalent L-C series network have been already calculated in Section 2. The equivalent circuit of this filter, as explained in Section 3, consists of the cascade connection of L-C series networks and ideal impedance inverters. Given the electrical specifications of the 5th-order filter ($f_0 = 3$ GHz, $RL = 25$ dB, $BW = 150$ MHz), the following values (in Ω) of the impedance inverters can be readily deduced: $K_{01} = K_{56} = 68.658$, $K_{12} = K_{45} = 14.387$, $K_{23} = K_{34} = 10.083$.

5.1 Design of the coaxial excitation

First, the design of the coaxial excitation of the input/output resonators of the bandpass filter is addressed. The dimensions of the coaxial waveguide ($\epsilon_r = 2.2$) are the same ones used in the 3rd-order filter (external and internal radii of 2.05 and 0.65 mm, respectively). In order to characterize the external quality factor Q_{ext}, we follow the same method explained for the 3rd-order filter. In this case, since the required quality factor is $Q_{ext} = 15.921$, an initial value of $d = 5.053$ mm can be deduced from Fig. 6.

5.2 Inter-resonator coupling

The inter-resonator couplings depend on the separation $s_{i,j}$ between the resonator strips (see Fig. 12). The required electromagnetic couplings between resonators can be computed as:

$$k_{1,2} = \frac{K_{1,2}}{w_0 \cdot L} = 0.0487 \tag{3}$$

$$k_{2,3} = \frac{K_{2,3}}{w_0 \cdot L} = 0.0341 \tag{4}$$

Therefore, the following initial values for the separation between resonators can be deduced from Fig. 7: $s_{1,2} = 19.236$ mm and $s_{2,3} = 22.551$ mm.

5.3 Systematic design using a step-by-step procedure

Once we have obtained a set of initial values for the relevant dimensions, we continue our filter design following a step-by-step strategy. The design process is based on the segmentation of the filter, where the different resonators are added one after the other,

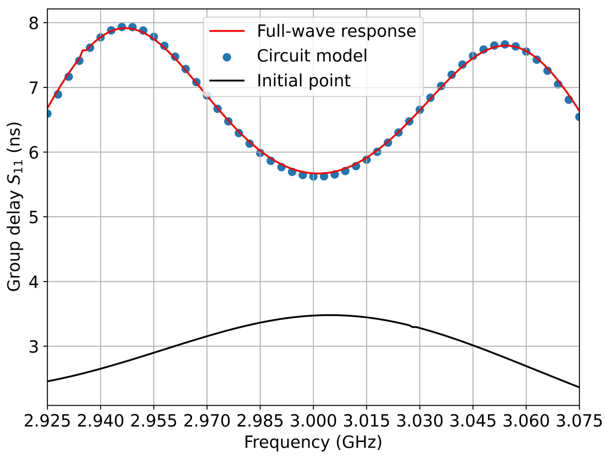

Figure 13. Electrical response of the waveguide structure considered in the first stage compared to the ideal response.

with the aim of reducing the number of variables to be optimized in each stage. The electrical response of the lumped-element equivalent circuit of the structure used in each step will be used as the target response. The optimized dimensions obtained in each step will then be used as initial values in the next step of the design process. This design procedure will be concluded with the ASM technique. All the simulations discussed in the next sections have been performed in a low-precision space using the EM software FEST3D.

5.3.1 First stage

In the first step of the design process, the component under consideration consists of the first two resonators of the interdigital filter (see Fig. 12) fed by a coaxial probe. It is worth noting that there is only one access port in this structure. The equivalent circuit of this waveguide component consists of the cascade connection of the input transmission line, inverter $K_{0,1}$, an L-C series network representing the first resonator, impedance inverter $K_{1,2}$, and another L-C series network short-circuited at its end. In this first stage, the dimensions to be optimized are the heights H_1 and H_2 of the strips, the separation $s_{1,2}$ between resonators, and the height d of the feeding probe (see Fig. 12). In this first stage, the set of dimensions obtained in the previous sections are used as a starting point in the optimization process.

Next, the dimensions of the waveguide component are optimized using, as a target response, the group delay of the S_{11} parameter of the circuit model. The results of the optimization are shown in Fig. 13, where a very good agreement can be observed between both set of data. The values obtained (in mm) for each dimension at the end of the optimization process are: $H_1 = 22.942$, $H_2 = 22.205$, $s_{1,2} = 19.059$ and $d = 4.522$. On the other hand, the set of initial dimensions used as a starting point in this first stage are: $H_1 = H_2 = 23.233$, $s_{1,2} = 19.236$ and $d = 5.053$ (the response of this initial point has also been included in Fig 13). As we can see, the optimized final values are, indeed, very close to the initial values.

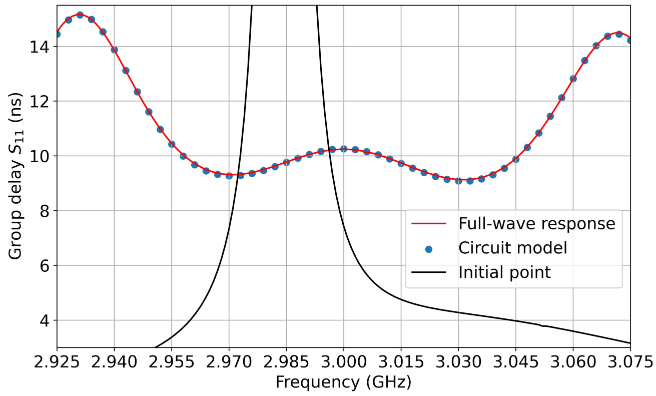

Figure 14. Electrical response of the waveguide structure considered in the second stage compared to the ideal response.

5.3.2 Second stage

In the second stage of the design process, a new resonator is added to the structure, thus obtaining a waveguide structure composed of the first three resonators of the filter (see Fig. 12). The circuit model of this structure can be readily obtained by adding to the circuit network of the previous step, the inverter $K_{2,3}$, and a new L-C series network. Next, the dimensions of this waveguide structure must be optimized to obtain the same electrical response of the ideal network. The parameters to be optimized in this stage are the same as in the previous step (H_1, H_2, $s_{1,2}$ and d), including also the height H_3 of the third resonator, and the separation $s_{2,3}$ between the second and third resonators (see also Fig. 12). The results of this optimization are shown in Fig. 14, where an excellent agreement is again observed between the response of the lumped-element model and the full-wave simulation. The final values (in mm) for the optimized dimensions are: $H_1 = 22.955$, $H_2 = 20.108$, $H_3 = 21.994$, $s_{1,2} = 22.226$, $s_{2,3} = 25.176$ and $d = 4.382$. The corresponding starting points are the final values obtained at the end of the previous stage. We have also included in Fig. 14 the response of the initial point from where the matching to the group delay reference curve is performed.

5.3.3 Third stage

At this point of the procedure, we have completed the design of one half of the bandpass filter, since the component is symmetrical. Therefore, the optimization of the whole filter can be performed next by taking into account that (see Fig. 12): $H_1 = H_5$, $H_2 = H_4$, $s_{1,2} = s_{4,5}$ and $s_{2,3} = s_{3,4}$. In this final stage of the design process, the S-parameters of the equivalent lumped-element network of the 5th-order filter are used as the target response, and all the dimensions of the structure are optimized. The optimization results are shown in Fig. 15, where an excellent agreement is observed between the full-wave EM-simulation, and the response of the ideal network, thereby validating the systematic design procedure proposed in this work. The final dimensions (in mm) of the filter (obtained in a low-precision space) are: $H_1 = H_5 = 22.960$, $H_2 = H_4 = 20.099$, $H_3 = 20.069$, $s_{1,2} = s_{4,5} = 22.198$, $s_{2,3} = s_{3,4} = 28.463$ and $d = 4.382$.

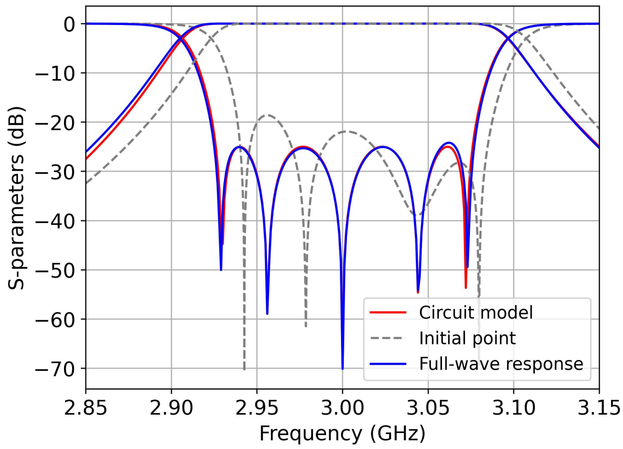

Figure 15. S-parameters of the 5th-order interdigital filter (coarse model) and response of the coarse model filter in the high-precision space (label: initial point).

5.4 Implementation of the ASM Technique

As already mentioned, all previous simulations have been performed in a low-accuracy space (using FEST3D). To continue, therefore, the final dimensions obtained in the previous section need to be mapped to a high-precision space using the ASM method. In this context, we have included in Fig. 15 the filter response in the high-precision space using the optimum dimensions designed in the coarse space.

Fig. 16 shows the frequency response of the filter after implementing the ASM technique. Again, two different EM simulators (Ansys HFSS and CST Studio Suite) have been used to validate the design process, obtaining an excellent agreement between both set of simulated data. In addition, the electrical response of the filter designed in the low-accuracy simulation space has also been included in Fig. 16. The values (in mm) of the dimensions of the 5th-order interdigital filter (after implementing the ASM technique) are: $H_1 = H_5 = 23.100$, $H_2 = H_4 = 20.204$, $H_3 = 20.174$, $s_{1,2} = s_{4,5} = 21.839$, $s_{2,3} = s_{3,4} = 28.059$ and $d = 4.421$.

Finally, we have compared in Table 1 the electrical performance of the bandpass filters designed in this work (3rd and 5th-order filters) with other similar designs (found in the technical literature) concerning interdigital waveguide bandpass filters using resonator posts with a cylindrical or a rectangular geometry.

6 Multipactor breakdown prediction

A power handling capability study of the designed interdigital filters is addressed in this section. In particular, the high-power performance of both topologies of interdigital filters discussed in this work (based on cylindrical posts and on flat strips) will be compared. The multipactor effect is a high-power phenomenon that appears in components used in communication satellites, under high vacuum conditions and in the presence of high-intensity electromagnetic fields, linked to an electron avalanche effect (Vaughan, 1988). This phenomenon can lead to a degradation of the device performance, so it is very important to properly characterize the behaviour of the designed components under high-power conditions.

In this context, Fig. 17 shows the electric field distribution in the 5th-order interdigital filter based on flat strips computed at $f_0 = 3$ GHz (with values scaled for an in-

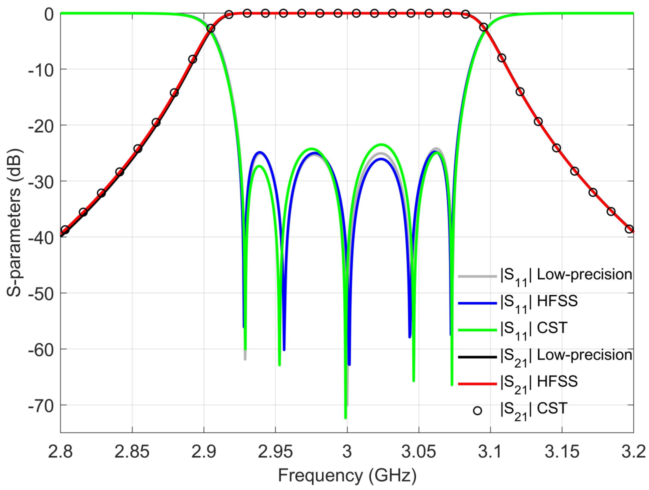

Figure 16. S-parameters of the 5th-order interdigital bandpass filter in the high-precision space. Comparison of results obtained with Ansys HFSS and CST Studio Suite.

Table 1. Electrical performance of several interdigital waveguide bandpass filters found in the technical literature.

Ref.	f_0 (GHz)	N	BW (GHz)	RL (dB)	Post geometry
This work	3	3	0.2	25	Rect.
This work	3	5	0.2	25	Rect.
(Packiaraj et al., 2005)	0.975 - 1.825	3	0.25 / 0.35	15	Cyl.
(Ikram & Rana, 2006)	6.175	5	0.5	10	Cyl.
(Munina & Turalchuk, 2015)	2.91 – 3 – 3.09	3	$\simeq$ 0.04 – 0.04 - 0.04	20	Cyl.
(J. Li et al., 2018)	15	8	4.4	10	Cyl.
(Wu et al., 2019)	14	4	1.4	15	Rect.
(Jiang et al., 2019)	11.725	8	2.05	17	Rect.
(Rodriguez-Morales et al., 2021)	3.75	11	2	10	Rect.
(Rodriguez-Morales et al., 2021)	6	11	2	10	Rect.
(Kong et al., 2023)	3.8	4	0.9	18	Rect.

put power level of 1 W). The electric field distribution reveals a high concentration of the electric field around all the metallic strips. Typically, the critical areas in terms of multipactor effect for classical interdigital resonators based on cylindrical posts are the zones between the top surface of the post and the top/bottom walls of the rectangular enclosure. Nevertheless, for the novel resonators based on planar strips proposed in this work, since the thickness of the strip used in our designs is small (only 1 mm), the equivalent capacitance in this region is less significant than the one found in classical resonators based on cylindrical posts. Therefore, a multipactor analysis in several isolated regions of the designed filters is required to identify the critical zones in this new filter topology.

After analysing the evolution of the electrons trajectory in the designed filters, we have identified that the critical areas in these structures are the flat surfaces of the first and last resonator strips facing the front and back walls of the rectangular enclosure (where the distance is of 3 mm). In these zones, there is, indeed, a large capacitance (probably the largest in the whole structure), thus becoming the most critical regions in terms of the multipactor phenomenon. This fact has to be taken into account if these filters are to be used in space applications, since, under vacuum conditions, they will be susceptible to resonant electron discharges.

Next, a power analysis of the interdigital filters designed in this work (considering that they have been manufactured in aluminium) has been performed under vacuum conditions using the commercial software Spark3D (which is part of CST Studio Suite). To do this, we have first used Ansys HFSS to compute the EM fields at the central frequency of the designed filters ($f_0 = 3$ GHz in all cases), and also at the frequencies (f_1 and f_2) where the S_{21} parameter group delay and stored energy are maximum. Next, the calculated EM fields are imported by the Spark3D simulator, which is used to estimate the multipactor power threshold (P_{th}) of the designed filters. A homogeneous electron seeding of 10000 initial electrons has been defined in the simulations. In addition, the main parameters of the SEY curve are: $\delta_{\max} = 2.92$, $\delta_0 = 0.8$, $E_1 = 17$ eV and $E_{max} = 276$ eV (ESA-ESTEC, E. P. D., 2020).

The obtained results for the 3rd-order interdigital filter based on flat strips are ($f_1 =$ 2.86 GHz, $f_2 = 3.15$ GHz): $P_{th,f_0} = 170$ W, $P_{th,f_1} = 72.8$ W and $P_{th,f_2} = 83.5$ W. Moreover, for the 5th-order interdigital filter we have obtained ($f_1 = 2.91$ GHz, $f_2 =$ 3.09 GHz): $P_{th,f_0} = 100$ W, $P_{th,f_1} = 45.4$ W and $P_{th,f_2} = 51.3$ W. Although the obtained multipactor power thresholds are lower at frequencies f_1 and f_2, in practice, the frequency bandwidth of the employed signals do not usually reach such extreme values. The minimum of these computed P_{th} values would be the maximum operating power of each filter in space applications. If needed, solutions like the one proposed in (Coves et al., 2023) can be used to increase these values.

In order to compare the power handling capability of the new proposed topology with that of the classical solution based on cylindrical posts, a multipactor analysis has also been performed for the designed 3rd-order interdigital filter based on cylindrical resonators. The obtained results are ($f_1 = 2.83$ GHz, $f_2 = 3.17$ GHz): $P_{th,f_0} = 79.4$ W, $P_{th,f_1} = 40.9$ W and $P_{th,f_2} = 31.4$ W. Therefore, compared to the data obtained for the 3rd-order filter based on flat strips, we can conclude that the new proposed topology exhibits a better high-power performance than the classical interdigital filters based on cylindrical resonators.

7 Conclusion

A systematic procedure for the efficient design of a new topology for interdigital bandpass filters, based on flat metallic strips, has been proposed. The design method combines the use of the classical circuit-based approach and a strategy based on the seg-

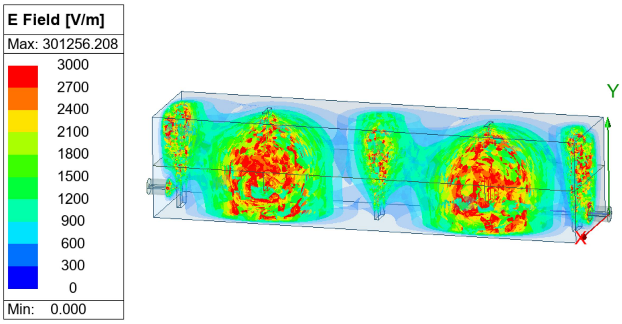

Figure 17. Electric field ($f_0 = 3$ GHz) in the 5th-order interdigital bandpass filter.

mentation of the filter, with the aim of reducing the number of variables to be optimized at each stage of the design process. Moreover, the ASM technique has been used in order to perform most of the simulations in a low-accuracy space, thus reducing the overall computational effort. Two interdigital bandpass filters operating in the S-band have been designed, and their electrical responses have been successfully compared to the results provided by two different EM full-wave simulators, thus validating both the new topology and the design procedure proposed. In addition, a multipactor study has been performed, in order to characterize the power capability of the components under vacuum conditions, in view of a possible use of the designed filters in satellite payloads. Finally, the design of a 3rd-order interdigital filter based on cylindrical posts has also been discussed. Our results have shown that the topology based on flat strips is as compact as the classical topology based on cylindrical post resonators, while exhibiting an enhanced broadband performance and a better power handling capability.

Open Research Section

Data were not used nor created for this research. The simulation results were obtained using ANSYS High Frequency Structure Simulator (ANSYS, 2024) and CST Studio Suite (Dassault Systemes, 2024).

Acknowledgments

This work has been funded by the Ministerio de Ciencia, Innovación y Universidades (Spanish Government) through the Subprojects C41 and C43 of the R&D Projects PID2022-136590OB (under grant AEI/10.13039/501100011033/FEDER, UE) and TED2021- 129196B (under grant 10.13039/501100011033/Unión Europea NextGenerationEU/PRTR), and in part by Conselleria de Educación, Universidades y Empleo, Generalitat Valenciana, under Project CIAICO/2021/055.

References

Anand, A. (2021). Cross coupling in folded interdigital filters using quarter-wavelength resonators with non-planar structures. In *2021 IEEE MTT-S International Microwave Symposium (IMS)* (p. 188-191).

ANSYS. (2024). *High Frequency Structure Simulator (HFSS).* Retrieved from `https://www.ansys.com`

Arndt, F., & Brandt, J. (2002). MM/FE CAD and optimization of rectangular combline filters. In *2002 32nd European Microwave Conference* (p. 1-4).

Bandler, J., Biernacki, R., Chen, S., Hemmers, R., & Madsen, K. (1995). Electromagnetic optimization exploiting aggressive space mapping. *IEEE Transactions on Microwave Theory and Techniques*, *43*, 2874-2882.

Bastioli, S., Snyder, R. V., & Macchiarella, G. (2018). Design of in-line filters with strongly coupled resonator triplet. *IEEE Transactions on Microwave Theory and Techniques*, *66*(12), 5585-5592.

Berenguer, A., Coves, A., Mesa, F., Bronchalo, E., & Gimeno, B. (2019). Analysis of multipactor effect in a partially dielectric-loaded rectangular waveguide. *IEEE Transactions on Plasma Science*, *47*(1), 259–265.

Boni, E., Giannetti, G., Maddio, S., & Pelosi, G. (2023). An equation-based method for the design of end couplings in combline microwave cavity filters. In *2023 IEEE International Symposium on Antennas and Propagation and USNC-URSI Radio Science Meeting (USNC-URSI)* (p. 1473-1474).

Cameron, R. J., Kudsia, C. M., & Mansour, R. R. (2018). *Microwave filters for communication systems.* Wiley.

Conciauro, G., Guglielmi, M., & Sorrentino, R. (2000). *Advanced modal analysis.* John Wiley.

Coves, A., Bonte, S., Morales, A., Vague, J., Boria, V., & Montero, I. (2023). Significant reduction of multipactor effect in a rectangular waveguide with periodically grooved metallic surfaces. In *1st ESA Space Microwave Week 2023* (p. 1-6).

Dassault Systemes. (2024). *CST Studio Suite.* Retrieved from `https://www.cst.com/products/csts2`

ESA-ESTEC, E. P. D. (2020). *Multipacting design test* (Tech. Rep.). Noordwijk, The Netherlands: European Cooperation for Space Standarization (ECSS).

García, R., Goni, J., Esteras, M., Tapia, R., & Montero, J. M. (2018). Filters developed at TRYO Aerospace for MetOP second generation mission. In *Proceedings of the 7th International Workshop on Microwave Filters* (p. 1-4). ESA/ESTEC, Noordwijk, The Netherlands.

Ikram, S., & Rana, I. E. (2006). Simulation and optimization of interdigital filter using serenade and HFSS. In *2006 IEEE International Multitopic Conference* (p. 111-115).

Jamshidi-Zarmehri, H., San-Blas, A. A., Neshati, M. H., Cogollos, S., Sharma, A., Boria, V. E., & Coves, A. (2023). Efficient design procedure for combline bandpass filters with advanced electrical responses. *IEEE Access*, *11*, 52168-52184.

Jiang, S., Wang, X., & Sun, L. (2019). Improved design of Ku-band interdigital cavity filter. In *2019 International Applied Computational Electromagnetics Society Symposium - China (ACES)* (p. 1-2).

Kobrin, K., Rudakov, V., Sledkov, V., Zimeng, L., & Manuilov, M. (2019). A novel design of wideband diplexer for base station applications. In *2019 Radiation and Scattering of Electromagnetic Waves (RSEMW)* (p. 148-151).

Kong, C., Wu, Z., & Hu, J. (2023). Design of a miniaturized interdigital cavity filter. In *2023 IEEE 11th Asia-Pacific Conference on Antennas and Propagation (APCAP)* (Vol. 1, p. 1-2).

Li, J., Huang, G., Yuan, T., Xu, J., & Li, H. (2018). A Ku-band wideband 3-D printed interdigital bandpass filter free of post fabrication tuning. In *2018 IEEE International Symposium on Antennas and Propagation and USNC/URSI National Radio Science Meeting* (p. 1439-1440).

Li, Z., Rudakov, V., Sledkov, V., & Zemlyakov, V. (2023). Compact UHF diplexer on multi-conductor coaxial cavity resonators. In *2023 Radiation and Scattering of Electromagnetic Waves (RSEMW)* (p. 184-187).

Macchiarella, G., Bastioli, S., & Snyder, R. V. (2018). Design of in-line filters with transmission zeros using strongly coupled resonators pairs. *IEEE Transactions on Microwave Theory and Techniques*, *66*(8), 3836-3846.

Macchiarella, G., Tamiazzo, S., Bastioli, S., & Snyder, R. V. (2023). Synthesis of strictly inline filters with transmission zeros. *IEEE Transactions on Microwave Theory and Techniques*, *71*(1), 274-284.

Matthaei, G., Young, L., & Jones, E. (1980). *Microwave filters, impedance-matching networks, and coupling structures.* Artech House.

Munina, I., & Turalchuk, P. (2015, 11). Low loss triplexer design for high power application in radars. In *2015 Loughborough Antennas & Propagation Conference (LAPC)* (p. 1-3).

Packiaraj, D., Ramesh, M., & Kalghatgi, A. (2005). Cavity diplexer using tapped line interdigital filters. In *2005 Asia-Pacific Microwave Conference Proceedings* (Vol. 1, p. 1-3).

Rodriguez-Morales, F., Brown, B., Sutton, A., Leu, M., Liou, F., Garrison, S., & Wolf, A. (2021). Additively manufactured interdigital filters for ultra-wideband radar. In *2021 IEEE Radio and Wireless Symposium (RWS)* (p. 137-140).

San-Blas, A., Coves, A., Vidal, A., & Boria, V. (2021). Efficient design of compact H-plane rectangular waveguide band-pass filters with integrated coaxial excitation. *AEU - International Journal of Electronics and Communications*, *135*, 153744.

Tamiazzo, S. (2021). Compact one-piece coaxial in-line comb filters and duplexers with transmission zeros. In *2021 IEEE MTT-S International Microwave Filter Workshop (IMFW)* (p. 284-287).

Thomas, J. (2003). Cross-coupling in coaxial cavity filters - A tutorial overview. *IEEE Transactions on Microwave Theory and Techniques*, *51*(4), 1368-1376.

Vallerotonda, P., Pelliccia, L., Tomassoni, C., Cacciamani, F., Sorrentino, R., Galdeano, J., & Ernst, C. (2019). Compact waveguide bandpass filters for broadband space applications in C and Ku-bands. In *2019 European Microwave Conference in Central Europe (EuMCE)* (p. 116-119).

Vaughan, J. (1988, 7). Multipactor. *IEEE Transactions on Electron Devices*, *35*, 1172-1180.

Venter, J. J. P., Maharaj, R., & Stander, T. (2020). Additive manufacturing of interdigital filters with arbitrary line cross section. *IEEE Transactions on Components, Packaging and Manufacturing Technology*, *10*(4), 686-693.

Wang, Y., & Yu, M. (2009). True inline cross-coupled coaxial cavity filters. *IEEE Transactions on Microwave Theory and Techniques*, *57*(12), 2958-2965.

Wu, R., Li, P., & Chu, R. (2019). Research on a new method to improve design flexibility and performance of interdigital cavity filter. In *2019 International Applied Computational Electromagnetics Society Symposium - China (ACES)* (Vol. 1, p. 1-2).

Yan, J.-J., Chen, F.-C., Xiang, K.-R., & Tu, Z.-H. (2024). Design of tunable coaxial bandpass filters with constant absolute bandwidth using one tuning element. *IEEE Transactions on Circuits and Systems II: Express Briefs*, *71*(4), 1959-1963.

Zeng, Y., Che, C., Yu, M., Lu, D., Cai, J. J., & Tan, Z. P. (2023). Novel miniaturized light-weight coaxial cavity filters with electrical mainline couplings. *IEEE Journal of Microwaves*, *3*(3), 1040-1050.

Zeng, Y., Yang, Y., Yu, M., & Bastioli, S. (2022). Synthesis of generalized strongly coupled resonator triplet filters by regulating redundant resonant modes. *IEEE Transactions on Microwave Theory and Techniques*, *70*(1), 864-875.